Infrared Spectroscopic Discrimination between the Loop and α-Helices and Determination of the Loop Diffusion Kinetics by Temperature-Jump Time-Resolved Infrared Spectroscopy for Cytochrome *c*

Manping Ye,* Qing-Li Zhang,* Heng Li,* Yu-Xiang Weng,* Wei-Chi Wang,* and Xiang-Gang Qiu†
*Laboratory of Soft Matter Physics and †Laboratory for Superconductivity, Beijing National Laboratory of Condensed Matter Physics, Institute of Physics, Chinese Academy of Sciences, Beijing 100080, China

ABSTRACT The infrared (IR) absorption of the amide I band for the loop structure may overlap with that of the α-helices, which can lead to the misassignment of the protein secondary structures. A resolution-enhanced Fourier transform infrared (FTIR) spectroscopic method and temperature-jump (T-jump) time-resolved IR absorbance difference spectra were used to identify one specific loop absorption from the helical IR absorption bands of horse heart cytochrome *c* in D_2O at a pD around 7.0. This small loop consists of residues 70–85 with Met-80 binding to the heme Fe(III). The FTIR spectra in amide I′ region indicate that the loop and the helical absorption bands overlap at 1653 cm^{-1} at room temperature. Thermal titration of the amide I′ intensity at 1653 cm^{-1} reveals that a transition in loop structural change occurs at lower temperature ($T_m = 45°C$), well before the global unfolding of the secondary structure ($T_m \approx 82°C$). This loop structural change is assigned as being triggered by the Met-80 deligation from the heme Fe(III). T-jump time-resolved IR absorbance difference spectra reveal that a T-jump from 25°C to 35°C breaks the Fe-S bond between the Met-80 and the iron reversibly, which leads to a loop (1653 cm^{-1}, overlap with the helical absorption) to random coil (1645 cm^{-1}) transition. The observed unfolding rate constant interpreted as the intrachain diffusion rate for this 16 residue loop was $\sim 3.6 \times 10^6$ s^{-1}.

INTRODUCTION

The amide I infrared (IR) absorbance, originating mainly from the amide C=O stretch vibrations of the peptide backbone (1–3), is an established indicator of the secondary and tertiary structures of proteins because of its sensitivity to hydrogen bonding, dipole-dipole interactions, and geometry of the peptide backbone (2,4,5). This broad multicomponent band contains contributions from the entire polypeptide backbone (α-helix, β-sheets, loops, and random coils, etc.). However the overall amide I absorption band is rather featureless, and different spectral resolution-enhanced methods have been developed to resolve the secondary structural components (6–8). Due to the spectral overlap of the structural components, unequivocal determination of the protein secondary structures by the use of resolution-enhanced IR spectroscopy still encounters difficulties.

Compared to the IR absorption of the other secondary structures, the correlation of the IR absorption band around 1655 cm^{-1} has been well established with the presence of α-helix for a large number of proteins, which has seldom led to a controversial assignment (2,3,9,10). However exceptions have been reported. Wilder et al. have investigated the Fourier transform infrared (FTIR) spectra of the secondary structures for two marine recombinant proteins (11) in which they found that the proteins have a significant absorption band near 1656 cm^{-1}, which is typically assigned to α-helical or random structure for other proteins. However circular dichroism (CD) spectroscopy analysis of the same proteins did not show any evidence of an α-helical structure. By comparing the proteins with their homolog whose structures have been determined by x-ray crystallography and NMR showing absence of α-helical structure, the observed 1656 cm^{-1} absorption band was thus assigned to a large loop rather than the α-helical structure. This indicates that the IR absorption from loop structure can overlap with that from the α-helical absorption and can be easily neglected or go unnoticed, especially when proteins consist of both the α-helical and the loop structures.

Cytochrome *c* (cyt *c*) is a small, water-soluble protein consisting of both α-helices and loops. The protein has a single polypeptide chain organized into three major helices and three major ω-loops with a covalently bound ferric heme group (12). The heme group binds to the peptide through the six-coordinate, low-spin iron present in heme. The fifth and sixth axial positions of iron are occupied by a relatively weak bond between the iron and sulfur of Met-80 and a stronger bond between the iron and N_3 from His-18 (13,14). It has been found that the Met-80 ligation would stabilize the local conformation of the cyt *c* (15). The high-resolution crystal structure of oxidized horse heart cyt *c* (16) and the stability of its secondary structural components marked in different colors with increasing stability in a sequence as red, yellow, green, and blue (17) are illustrated in Fig. 1 (*upper panel*). The lower panel in Fig. 1 presents the structures of three major ω-loops with residue sequence of 70–85, 36–61, and 20–35, respectively. It has been shown that the structure of oxidized horse cyt *c* in solution appears to be similar to that

Submitted February 14, 2007, and accepted for publication May 31, 2007.

Address reprint requests to Yu-Xiang Weng, E-mail: yxweng@aphy.iphy.ac.cn.

Editor: Feng Gai.

0006-3495/07/10/2756/11 $2.00

doi: 10.1529/biophysj.107.106799

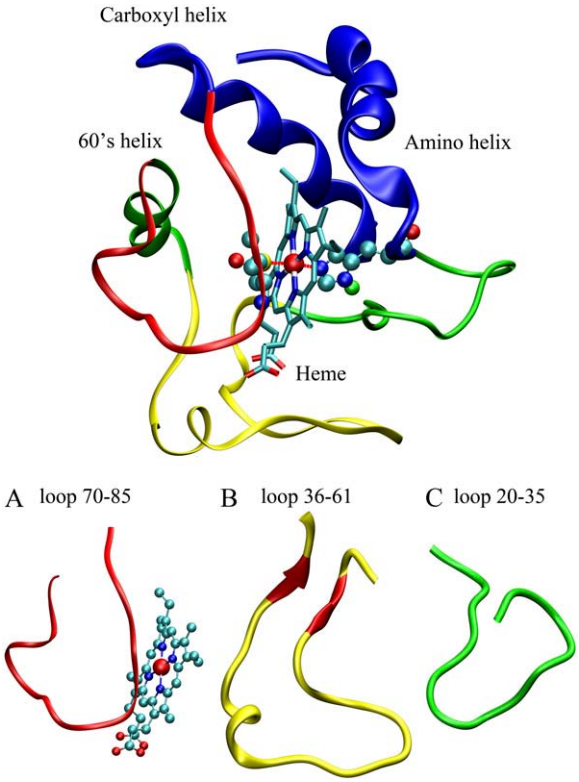

FIGURE 1 Schematic representation of the structure of horse heart cyt *c* and the three loop structural components based on the high-resolution crystal structure of oxidized horse heart cyt *c*. (*Upper panel*) Structure of horse heart cyt *c*. (*Lower panel*) Structures of three loops: (*A*) Small ω-loop 70–85 containing Met-80; (*B*) ω-loop from 36–61; and (*C*) ω-loop from 20–35. The thermal stability is marked in color with an increasing order of red<yellow<green<blue.

of the x-ray structure (18,19). The structural flexibility is considered to play a special role in the formation and dissociation of cyt *c* (20), which has been studied extensively by the use of molecular dynamics simulations and a variety of experimental methods (21–23), e.g., CD, fluorescence, and IR spectroscopy.

It has been shown that cyt *c* undergoes sequential cooperative unfolding of its secondary structural components (24). When increasing temperature or pH of the solution, some of the loop structures (*red* and *yellow* in Fig. 1) unfold before α-helices; in particular, the ω-loop containing Met-80, which is the most unstable structural unit, unfolds at a lower temperature. It has been found that weakening of the iron-sulfur bond by raising the pH at room temperature or by increasing the temperature at neutral pH is associated with the well-documented alkaline isomerization, where the Met-80 ligand was replaced by one or more strong field ligand (25). FTIR spectroscopy has been used to investigate the thermally induced conformation change of cyt *c*. By tracing the amide II intensity of the buried peptide NH protons in D_2O (1525–1560 cm^{-1}), which comprises primarily the NH bending of peptide groups, the result shows a tertiary structural transition at 54°C. This transition occurs well before loss of the secondary structure and is assigned to the protein conformational change induced by the Met-80 heme-ligand exchange (26).

The folding paths of cyt *c*, especially the ultrafast kinetic phase (submicrosecond) is still under intensive investigation (27). The ultrafast folding kinetics of cyt *c* has been studied mainly in its reduced form, i.e., ferrocytochrome *c*, by use of the photoinitiation mechanism of Jones et al. (28), which involves photodissociation of the CO complex of cyt *c* partially denatured in guandidine HCl (GuHCl). Photolysis is expected to trigger folding because the protein is destabilized by displacement of the native ligand Met-80 by exogenous CO at the heme Fe(II) axial coordination site (29). Since photodissociation of CO occurs in subpicosecond times (30), there is virtually no dead time in probing the dynamics of the refolding peptide. The presence of the heme renders possible the use of a variety of spectroscopic probes in the time-resolved mode in the Soret band including optical spectroscopy and magnetic CD (29,31). In the optical absorption-probed photolysis experiment, the sensitivity of the Soret band to heme ligation facilitates the detection of methonine or histidine ligation to the heme Fe(II), which enables the probe of the diffusive intrachain dynamics. To the authors' knowledge, direct probe of the secondary structural change reflecting the intrachain diffusion in cyt *c* has not been reported yet.

In contrast to the optical absorption in the visible region, mid-IR spectra can probe the protein secondary structures. The temperature-jump (T-jump) method can initiate a thermally induced protein unfolding process with a time-resolution as high as 70 ps (32). The T-jump method combined with the time-resolved IR absorbance difference spectra are well established for the study of ultrafast protein folding/unfolding dynamics (33,34). The T-jump method provides a means to quickly perturb the temperature of the system and shift the equilibrium position of the folded/unfolded state. The relaxation to the new equilibrium position corresponding to the elevated temperature is monitored by the time-resolved amide I′ (the prime denotes the frequencies of deuterated amide groups) absorbance of the polypeptide backbone. Here we report the investigation on differentiating amide I′ absorption of the loop from that of the helices for the deuterated oxidized horse cyt *c* by means of temperature-dependent FTIR difference spectra. We further studied the folding/unfolding kinetics of the loop dissociation associated with the methionine deligation from the heme Fe(III), in which a intrachain diffusion time constant of the loop at a submicrosecond timescale was determined. The ability to trace the ultrafast secondary structural transition during the T-jump-induced deligation of methionine from heme Fe(III) distinguishes this work from earlier studies that employed Soret band absorption of heme as the probe for the ultrafast intrachain diffusion (28,31).

MATERIALS AND METHODS

Chemicals

Horse heart cyt *c* (c-7752) was purchased from Sigma (St. Louis, MO) and used without further purification.

FTIR spectroscopy

FTIR absorbance spectra of cyt *c* at various temperatures were collected on an ABB-BOMEM FTIR spectrometer (ABB-BOMEM, Bureau, Québec) equipped with a liquid nitrogen cooled broadband mercury cadmium telluride (MCT) detector. Horse heart cyt *c* for FTIR measurement was prepared by dissolving the cyt *c* in 99.9% D_2O at a pD around 7.0 and a concentration of 1 mM in an airtight bottle for 24 h. It has been noted that salt linkage to the carboxyl groups would alter the amide I′ frequency (35), thus we dissolved cyt *c* in D_2O instead of the corresponding buffer solution. It has been shown that cyt *c* in neutral or slightly basic water without buffer is still in its native state (36). Two mounted CaF_2 sample cells were filled with the sample solution and the reference D_2O using a Teflon spacer at an optical path length of 56 μm. To correct for slow instrument drift, a programmable translation stage was used to move both the sample and reference cells in and out of the IR beam, alternatively. Each spectrum was recorded in the amide I′ band at a resolution of 2 cm^{-1} and 300 scans were signal averaged.

To eliminate spectral interference from atmospheric water vapor, the measurement was performed in a vacuum chamber at a vacuum of 22 Pa in a specially designed chamber which allows the water flowing through vacuum-sealed pipes to maintain the samples at the desired temperature. The temperature was controlled to an accuracy within $\pm$0.25°C using a thermostat (Harrick, Pleasantville, NY). The spectra were taken every 2°C or 3°C between 25°C and 58°C, and every 5°C between 58°C and 93°C. The FTIR spectrum was collected after the sample was thermally equilibrated for 15 min. The reference D_2O spectra were recorded under the same condition. Reference spectral subtraction was carried out digitally to give a straight baseline in the spectral region of 1750 $\sim$ 2000 cm^{-1} (17). A linear baseline was subtracted from each spectrum.

Heating-and-cooling scan FTIR spectra were collected to examine the reversibility of folding/unfolding as well as the hydrogen/deuterium exchange processes for cyt *c* at different temperatures. Difference FTIR spectra were acquired between those before and after the sample was cycled to different elevated temperatures up to 60°C then returned to the room temperature. It is found that the FTIR spectra exhibit no changes when the sample was cycled to a temperature below 35°C, whereas the difference spectra between the cycled and noncycled samples show a small bleaching band at 1653 cm^{-1} when the cycling temperature is lower than 45°C. When the temperature is raised to 50°C or higher, a broad absorption amide I′ band spanning from 1605 to 1690 cm^{-1} with a peak at 1648 cm^{-1} appears. This multicomponent absorption is possibly due to the irreversible protein folding/unfolding as well as the hydrogen/deuterium exchange of the buried groups. Therefore we concluded that the hydrogen/deuterium exchange was almost completed for the exposed groups, which unfold at a temperature below 45°C, and the cyt *c* undergoes a completely reversible folding/unfolding process when the heated temperature is lower or around 35°C. Evidence of obvious aggregation was found at temperatures above 50°C ($\sim$6%).

IR-SD spectra

Second derivative spectrum is a resolution-enhanced method for spectral analysis (2,37). In this spectrum, the resulting peak frequencies would be identical to that of the original FTIR spectra; however the halfwidth of the band would be reduced by a factor of 2.7, which substantially increases the spectral resolution (2,37). In this work, the second derivative spectra were calculated using Savitsky-Golay derivative software.

T-jump and time-resolved IR difference absorbance spectra

The laser-induced T-jump technique and the time-resolved IR spectrometer have been described elsewhere (38). Briefly, a 1.9 μm heating pulse was generated via Raman shifting the 1064 nm fundamental output of a Nd:YAG laser (Lab 170, 10 Hz, 8–12 ns, Spectra Physics, Mountain View, CA) in a Raman cell filled with H_2 gas at a pressure of $\sim$50 atm. A liquid N_2 cooled continuous wave CO laser (Dalian University of Technology, Dalian, China) was employed as the IR probe source, which was tunable from 5.0 μm (2000 cm^{-1}) to 6.5 μm (1540 cm^{-1}). A single output wavelength can be selected within the CO vibration-rotation spectrum with an approximate spectral spacing of 4 cm^{-1} by tuning the angle of the grating inside the laser cavity.

The output wavelength was calibrated by an IR monochromator within an uncertainty of 2 cm^{-1}. The IR laser has a TEM00 mode from a 165 cm laser cavity with an average output power at a single wavelength around 20 mW. Compared to the previously widely used diode laser IR probe source, the CO laser has a much higher output power, wider tunable range, and possibly a better beam quality, rendering itself an excellent probe source for the study of T-jump-induced protein secondary structural changes in the amide I region. The IR probe beam was detected by a liquid N_2 cooled photovoltaic MCT detector (Kolmar, Newburyport, MA) equipped with a sensitive current preamplifier (Kolmar, KA020-A1), which has a band-pass of 20 MHz.

An accessible dynamic range is from $\sim$20 ns (limited by the detector rise time and laser pulse width after deconvolution of the instrumental response function) to $\sim$1 ms (when the solution starts to cool, where the monoexponential decay time constant for the thermal relaxation was $\sim$6 ms, depending on the magnitude of T-jump and the optical path length). The intensity of the transmitted IR probe beam and the corresponding transient absorbance change induced by the T-jump pulses represented by V_0 and ΔV, respectively, were recorded by a digital oscilloscope (Tektronix TDS520D, Santa Clara, CA). Both the signals were finally transferred to a PC for data analysis. The difference spectra were reconstructed by the optical difference between the T-jump-induced absorbance change of the sample and that of the reference D_2O. The calibration of the T-jump amplitude follows the reported protocols (39). Briefly, the T-jump-induced absorbance change of the reference D_2O at probing wavelength ν ($\Delta A(\Delta T,\nu)$) was measured, and the T-jump amplitude was estimated by the following equation: $\Delta A(\Delta T, \nu) = a(\nu)\Delta T + b(\nu)\Delta T^2$, where $\Delta T = T_f - T_i$ is the T-jump amplitude; T_f and T_i correspond to the final and initial temperature, respectively; and $a(\nu)$ and $b(\nu)$ are the fitting parameters determined by the FTIR spectra of D_2O measured at different temperatures (40). The instrumental temporal response of this system is $\sim$80 ns as determined by fitting the T-jump kinetics of the D_2O reference signal convoluted with a Gaussian instrumental response function, where the rising time constant for heating D_2O is set as 20 ns based on the pulse width of the Nd:YAG laser. If it is not stated otherwise, the time constants from the fitting of the experimental kinetics are deconvolved by the instrumental response function.

In the T-jump measurement, the CaF_2 sample cell was divided into two compartments with a 56-μm-thick Teflon sheet. One compartment was filled with the sample solution, whereas the other was filled with D_2O reference. The T-jump-induced absorbance difference measured when the two compartments were filled with D_2O was $\sim 5 \times 10^{-4}$ in optical density (OD) after averaging for 300 laser shots. However this detection limit was difficult to achieve for protein samples. The T-jump-induced absorbance change of proteins is very sensitive to the T-jump amplitude, and in this work the accuracy of the ΔT was within $\pm$1.5°C. Therefore, repeated experiments were conducted for the reproducibility of the presented T-jump-induced time-resolved IR absorbance difference spectra. To further confirm the reversibility of the folding as suggested by the reviewers, the folding/unfolding kinetics as well as the T-jump time-resolved difference IR spectra were conducted in a flowing cell of the same path length, in which both the sample and reference compartments were flowed with a peristaltic pump (Cole-Parmer, Vernon Hills, IL). The calculated minimum flow rate for having every laser shot heat the fresh sample is 23.6 μL/min. In the experiment, we kept a flow rate of 1 mL/min, well above the minimum requirement.

RESULTS AND DISCUSSION

Correlations between the amide I′ band positions and the secondary structure in proteins have shown that the band centered at ~1654 cm^{-1} corresponds to that of α-helices; 1629 and 1675 cm^{-1} bands to the low- and high-frequency of β-sheet structure; 1668, 1675, and 1686 cm^{-1} to turns; and a component at 1645 cm^{-1} to the disordered random coils (41,42). Fig. 2 *A* shows a series of selected FTIR spectra of cyt *c* in D_2O at different temperatures (from 25–93°C). From Fig. 2 *A*, it can be seen that as the temperature rises, the major broad band at 1653 cm^{-1} loses its intensity with a concomitant peak shift from 1653 to 1649 cm^{-1}, whereas the two bands at 1614 and 1684 cm^{-1} increased slightly, which can be assigned to the formation of the intermolecular antiparallel

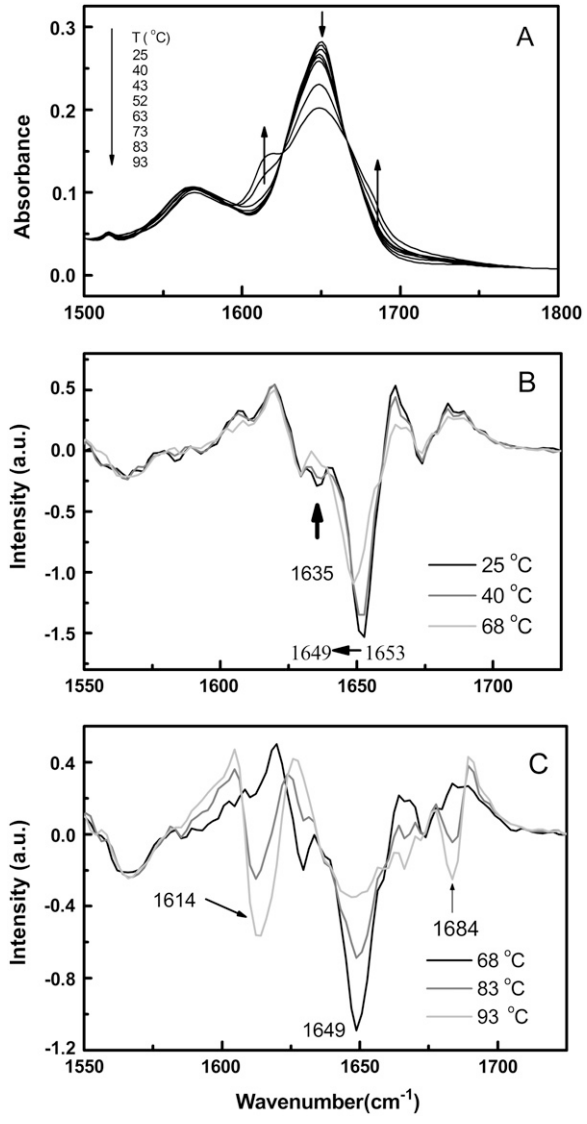

FIGURE 2 (*A*) FTIR absorption spectra of oxidized horse heart cyt *c* in D_2O, 1 mM (pD ~ 7.0) at different temperatures. Second derivative of FTIR absorption spectra for oxidized horse heart cyt *c* at different temperatures of (*B*) 25°C, 40°C, and 68°C and (*C*) of 68°C, 83°C, and 93°C, respectively.

β-sheets resulting from reversible or irreversible aggregation (43) depending on the temperature to which the sample is heated as discussed in the previous section.

Fig. 2, *B* and *C*, displays a series of typical second derivatives of the FTIR spectra over different temperature regions, i.e., 25–68°C (Fig. 2 *B*) and 68–93°C (Fig. 2 *C*). Fig. 2 *B* reveals clearly that at the lower temperature range the major band shifts from 1653 to 1649 cm^{-1} as temperature is increased. Fig. 2 *C* shows an increase in intensity of two new major bands appearing at 1684 and 1614 cm^{-1} with a simultaneous loss of intensity at 1649 cm^{-1} on further increase of temperature. Combining Fig. 2, *B* and *C*, the results reveal that the major peak shifts from 1653 to 1649 cm^{-1} as the temperature rises and it is stabilized at 1649 cm^{-1} at a temperature around 68°C or higher. This fact suggests that the structural component corresponding to the absorption band at 1653 cm^{-1} is less stable to thermal perturbation than that at 1649 cm^{-1}.

It has been assumed in the literature that the FTIR absorptivities of the secondary structural elements are the same, though some side chains also have absorptions in the amide I′ spectral region (44). We use the integrated area under the fitted band as a quantitative content indicator for the given secondary structure (3,18). We examined dependency of the total integrated area of the amide I′ band against the temperature. The result shows that although the amide I′ absorption band shape changes with the increasing temperature, the total integrated intensity drops by only ~1.3% when the temperature is raised from 25°C to 93°C. This fact justifies the validity of the above assumption in the case here. Fig. 3 plots thermal titration curves of cyto *c* at 1614, 1635, and 1653 cm^{-1}, respectively, from 4°C to 93°C.

On fitting the data in Fig. 3, *upper panel* and *middle panel*, with a two-state transition curve, the transition midpoint temperature (T_m) of the corresponding secondary structures associated to intermolecular aggregation and extended β-sheet was obtained as 82°C and 85°C for 1614 and 1635 cm^{-1} bands, respectively. These T_m values agree well with those for cyt *c* reported by Muga (45) and are interpreted as the T_m for two-state global unfolding of cyt *c*. A remarkable feature in Fig. 3, *bottom panel,* is that the curve can be fitted by two independent two-state transition curves with the first transition midpoint temperature at 45°C and the second at 82°C, respectively. Obviously the second transition process at higher temperature merges into the global unfolding process of cyt *c*; therefore the lower-temperature transition process should come from the unfolding of a less stable local structural segment.

It has been reported that when pD is changed from 7 to 11, the amide I′ peak shifts from 1652 cm^{-1} to 1648 cm^{-1} accompanied by an intensity loss. This has been suggested as the axial methionine bond to the iron being broken at a high pH value, thus lowering the structural integrity of the protein (35). NMR experiments have further established the interdependence between the pH- and temperature-induced local conformational changes occurring during the conversion of

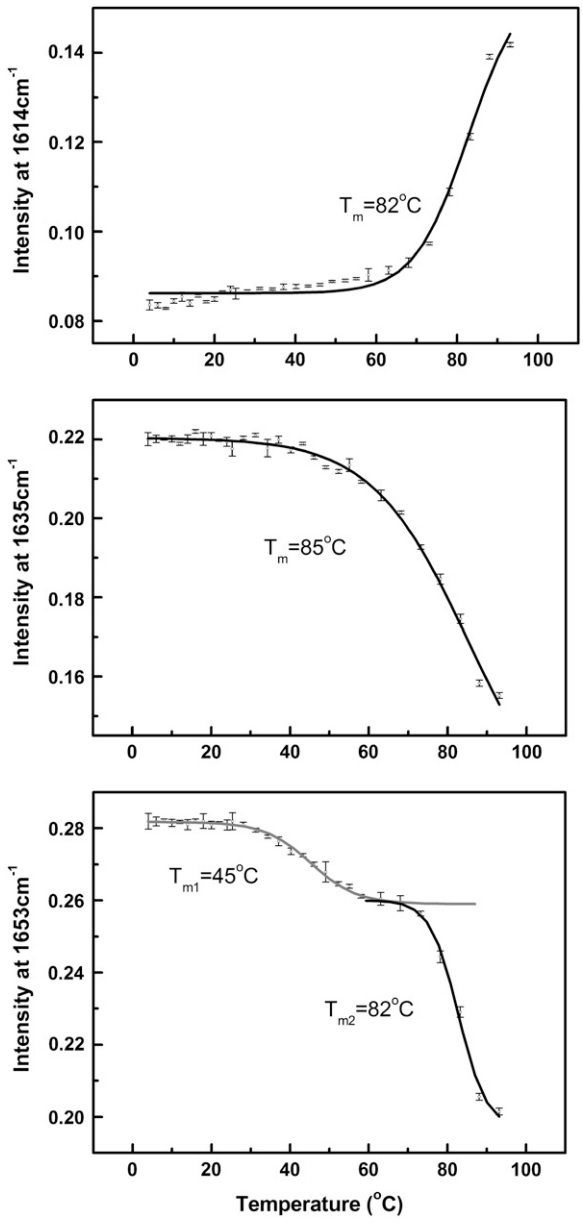

FIGURE 3 Thermal titration of amide I′ intensity for oxidized horse heart cyt *c* at (*top*) 1614 cm^{-1}, (*middle*) 1635 cm^{-1}, and (*bottom*) 1653 cm^{-1}. Open circles are the experimental data, and the solid line is the fitted curve. The 1614 and 1635 cm^{-1} data are fitted with a two-state transition model, which give similar transition midpoint temperatures (T_m) of 82°C and 85°C, respectively. The absorbance change at 1653 cm^{-1} is fitted by two independent two-state transition models with two transition midpoint temperature of 45°C (T_{m1}) and 82°C (T_{m2}), respectively.

native horse ferricytochrome *c* to its alkaline isomers (46). Apparently our observed lower transition midpoint at 1653 cm^{-1} band and the corresponding band shift coincide well to that observed pH-induced cyt *c* alkaline isomerization process. Therefore the observed thermally induced band loss at 1653 cm^{-1} in a lower temperature region should correspond to the thermal breaking of the iron-sulfur (Met-80) bond, leading to the unfolding of the small loop containing residues of 70–85. Thus we suggest that except for the α-helical absorption, an additional absorption component at 1653 cm^{-1} should come from the ω-loop containing Met-80. This is in agreement with the conclusion of the other study that the ω-loop containing Met-80 is the most unstable structural unit which unfolds at a lower temperature (24). Once this ω-loop unfolds, it lowers the integrity of the cyt *c* molecule, leading to a red shift of the helical absorption band.

To get an insight into the thermally induced unfolding process of cyt *c*, T-jump time-resolved IR difference absorbance spectra were employed to probe the unfolding process of the ω-loop containing Met-80 and its corresponding conversion to other secondary structural components. The unfolding process can be initiated by T-jump (24). This technique has also been used to study the unfolding of apomyglobin (47) and the folding/unfolding process of the other proteins (39). For a simple two-state kinetics, the observed relaxation rate is the sum of the forward and backward reaction rates, and each can be determined separately if the equilibrium constant is known (48). Fig. 4 *A* shows the T-jump time-resolved IR absorbance difference spectrum in amide I′ region recorded at 1.4 μs after the T-jump at 25°C with a ΔT of 10°C, and the difference FTIR absorption spectrum between 36°C and 25°C is also presented for comparison, which reveals that the envelope of the time-resolved transient difference IR spectrum is roughly coincident with that of the difference FTIR spectrum.

The T-jump time-resolved IR absorbance difference spectrum shows several bleaching peaks at 1634, 1651, and 1674 cm^{-1} and a main absorption peak at 1645 cm^{-1} in contrast to the broad-band spectrum with discernable peaks at 1635, 1653, and a shoulder at 1674 cm^{-1} in the difference FTIR spectra (the slight difference in the peak wavelength between the steady-date IR and time-resolved IR is caused by the CO probe laser since it delivers individual wavelength with a spacing around 4 cm^{-1}). The bleaching peaks indicate that a T-jump induces the unfolding kinetics of β-sheet (1635 cm^{-1}), ω-loop containing Met-80 (1651 cm^{-1}), and turn (1674 cm^{-1}) structures, whereas the absorption peaks indicate the folding kinetics of random coil (1645 cm^{-1}).

A striking difference between the T-jump time-resolved IR absorbance difference spectrum and that of the steady-state FTIR is that the absorption peak at 1645 cm^{-1} appearing in the former is missing in the latter. To further confirm that this absorption peak would not originate from the irreversible aggregation of the protein due to repeated laser shot, we conducted the T-jump experiment in a flowing cell. The T-jump time-resolved difference spectra of the sample under flowing and nonflowing conditions are compared in Fig. 4 *B*, where the result shows that the main spectral features are reproducible, excluding the possibility that this transient absorption comes from the irreversible unfolding of the protein. The 1645 cm^{-1} absorption peak lies between two neighboring bleaching peaks at 1635 and 1651 cm^{-1} in the T-jump time-resolved difference spectra. It is expected to appear also in the steady-state FTIR difference spectrum.

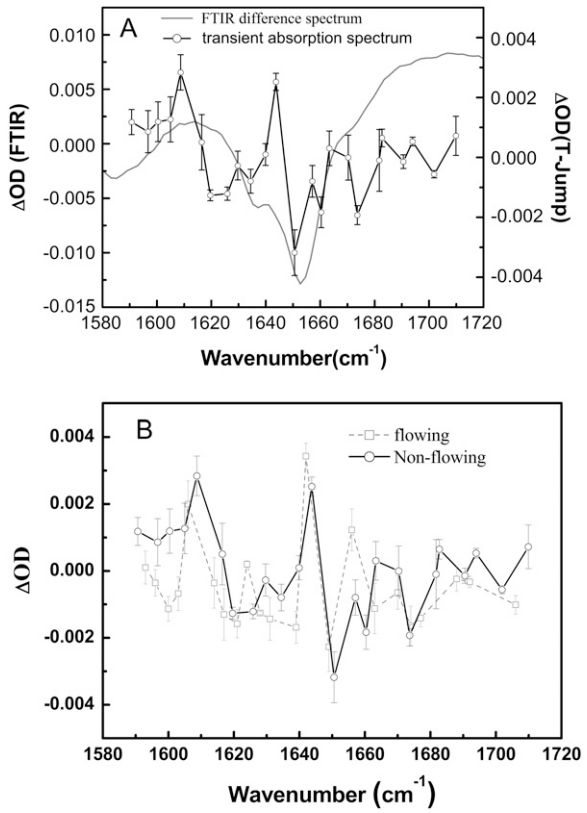

FIGURE 4 (*A*) Comparison of the FTIR absorbance difference spectrum (*shaded line*) between 36°C and 25°C with the T-jump (from 25°C to 35°C) time-resolved IR absorbance difference spectrum delayed at 1.4 μs (*open circles*) for the oxidized horse heart cyt *c*. The error bars were calculated based on three parallel measurements with the same sample. (*B*) Comparison of the T-jump (from 25°C to 35°C) time-resolved IR absorbance difference spectrum delayed at 1.4 μs for the oxidized horse heart cyt *c* acquired in the flowing and nonflowing cell.

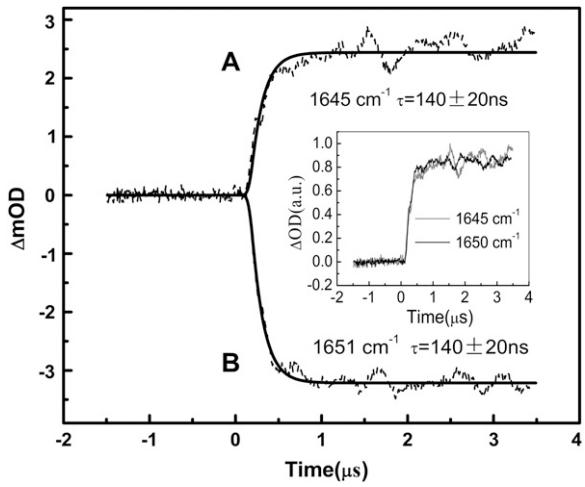

FIGURE 5 Kinetic IR response (*dashed lines*) of oxidized horse heart cyt *c* at two different probe wavelengths for a T-jump from 25°C to 35°C at 1645 cm^{-1} (*A*) and 1651 cm^{-1} (*B*). The solid curves represent fits of the experimental data to single-exponential kinetics convoluted with the instrument response function. The time constants are 140 ± 20 ns for both the kinetics. (*Inset*) Superimposing of kinetic trace at 1645 cm^{-1} (*shaded line*) with the inverted trace at 1651 cm^{-1} (*solid line*).

However, the spectral bands in the steady-state FTIR difference spectrum are broader, and there is a great chance that the positive absorbance at 1645 cm^{-1} would be offset by the two neighboring intense bleaching peaks leading to a dip at 1641 cm^{-1} riding on the bleaching envelope.

Fig. 5 presents the corresponding kinetics at the two typical bands, i.e., a bleaching recovery kinetics at 1651 cm^{-1} with a time constant of 140 ± 20 ns and an absorption kinetics at 1645 cm^{-1} with a time constant of 140 ± 20 ns for the rising phase fitted by a monoexponential equation. When the bleaching kinetics at 1651 cm^{-1} is inverted, it well matches that of the absorption kinetics at 1645 cm^{-1} as shown in the inset. This fact suggests that unfolding of the ω-loop containing Met-80 leads to the formation of a random coil structure (1645 cm^{-1}), i.e., the bleaching kinetics corresponds to the process of iron-sulfur bond dissociation and a cooperative unfolding of the ω-loop containing Met-80, whereas the absorption kinetics arises from the formation of the random coil structure generated by the unfolding of the ω-loop.

Fig. 6 presents the IR response kinetics detected at 1635 cm^{-1} after the T-jump, where the β-sheet absorption is expected. This kinetics can be resolved into two independent processes, i.e., a bleaching kinetics with a time constant of ~60 ± 20 ns with a relative amplitude of 60% and an absorption kinetics with a time constant ~280 ± 20 ns and a relative amplitude of 40%. Thus we assign the 60 ± 20 ns time constant to the unfolding of the β-sheet and the 280 ± 20 ns to the formation of the β-sheet from the other structural components. The bleaching phase with a time constant of 60 ± 20 ns is faster than that for the unfolding kinetics of the ω-loop containing Met-80. Therefore the unfolding process of β-sheet absorbing at 1635 cm^{-1} with a time constant of 60 ± 20 ns and the ω-loop at 1651 cm^{-1} are not cooperative within the observed temporal region.

When raising the initial temperature from 25°C to 40°C, the protein folding/unfolding equilibrium would shift toward a more unfolded state, especially for the most unstable ω-loop containing Met-80. Fig. 7 shows the time-resolved difference IR spectrum in which temperature jumps from 40°C to 50°C acquired in a nonflowing cell. Later it has been confirmed that the main spectral features can be reproduced in a flowing cell. The corresponding difference FTIR spectrum between the final and initial temperature was also given for comparison. Unlike Fig. 4 *A*, the time-resolved transient difference IR spectrum after T-jump shown in Fig. 7 is quite different from the steady-state difference FTIR spectrum. In the T-jump-induced time-resolved transient difference IR spectrum, there are two major peaks, one is the bleaching peak at 1675 cm^{-1} and the other is the absorption peak at 1655 cm^{-1}. These two peaks can be interpreted as the

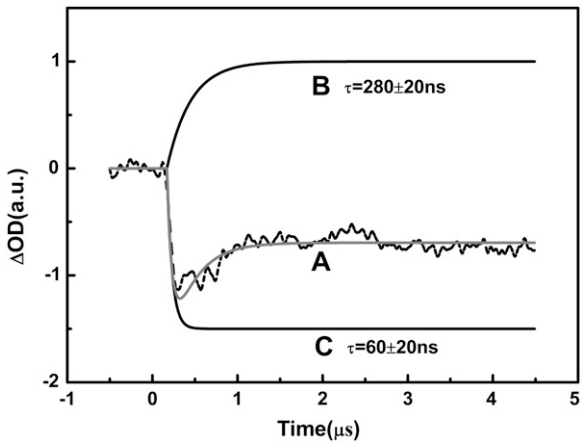

FIGURE 6 Kinetic IR response of oxidized horse heart cyt *c* at 1635 cm^{-1} with a T-jump from 25°C to 35°C (*A*, *solid line*). The corresponding fitting curve (*A*, *shaded line*) is a sum of two individual monoexponential processes: an absorption kinetics with a rise time constant of 280 ± 20 ns and a relative amplitude of 40% (*B*) and a bleaching process with a time constant ~60 ± 20 ns and relative amplitude of 60% (*C*).

unfolding of the β-turn and the formation of the loop structure. In the steady-state difference FTIR spectrum, there is one major bleaching peak at 1653 cm^{-1} together with a bleaching shoulder at 1636 cm^{-1}, which correspond to the unfolding of the ω-loop containing Met-80 or α-helices (1653 cm^{-1}) and the β-sheet (1636 cm^{-1}).

The difference between the time-resolved and the steady-state difference IR spectra can be interpreted as follows. The T-jump generated by the heating laser pulse can persist only for tens of milliseconds (with a decay time constant around 6 ms) before relaxation to the initial temperature and the T-jump-induced protein folding/unfolding processes are reversible at the short timescale. We have acquired the T-jump-induced folding/unfolding kinetics at millisecond timescale, and the results show that the transient signal returns to the background level when the initial temperature is recovered. In contrast, for the conventional heating process a constant thermal flow is employed to heat the system or keep the system at a constant temperature. This would induce some irreversible protein unfolding process especially at a higher temperature. As revealed by the FTIR difference spectra of scanning the temperature up and down, ~6% cyto *c* undergoes irreversible change when it is heated up to 50°C. Therefore the time-resolved difference IR spectra reflect the fast elementary steps comprising the folding/unfolding equilibrium on a short timescale, whereas the steady-state difference IR spectra comprise all the slow and fast, reversible and irreversible processes. Especially when the slow folding process dominates that of the fast process, the discrepancy between these two different kinds of difference spectra can be significant.

At a higher temperature, the protein folding/unfolding equilibrium shifts to the unfolded state, and the population ratio for the native state and the unfolded state can be inverted. It is expected that the unfolding process of the ω-loop containing Met-80 would become less prominent as that observed at lower temperatures. In addition, at higher temperatures other more stable secondary structures would begin to lose their stability, and the corresponding folding/unfolding kinetics would be complicated by folding/unfolding kinetics of several intermediate unfolded states, which gives rise to different spectral features in time-resolved IR absorbance difference spectra when the initial temperature for the T-jump is different.

Fig. 8 shows transient bleaching recovery kinetics in response to a T-jump from 40°C to 50°C probed at 1635 cm^{-1}, which is assigned to the β-sheet absorption (49). This

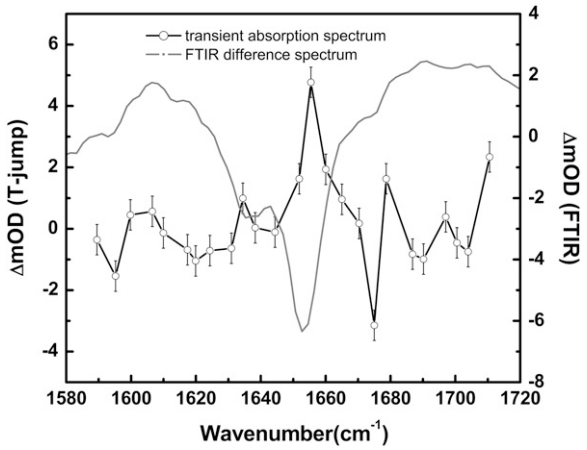

FIGURE 7 Comparison of the FTIR absorbance difference spectrum between 50°C and 40°C (*shaded line*) to the T-jump time-resolved IR difference absorption spectrum delayed at 1.4 μs with a T-jump from 40°C to 50°C (*open circles*) for the oxidized horse heart cyt *c*. Averaged error bars based on the resolution limit of the instrument were pasted.

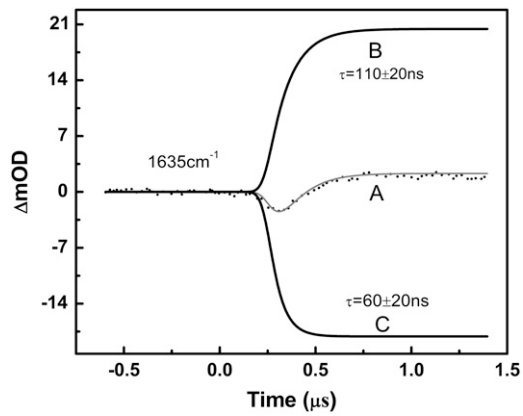

FIGURE 8 Kinetic IR response of oxidized horse heart cyt *c* at 1635 cm^{-1} with a T-jump from 40°C to 50°C (*A*, *dotted line*). The fitting curve (*A*, *shaded line*) is a sum of two monoexponential processes: an absorption kinetics with a rise time constant of 110 ± 20 ns and a relative amplitude of 53% (*B*) and a bleaching kinetics with a time constant ~60 ± 20 ns and relative amplitude of 47% (*C*).

kinetics can be resolved into two individual dynamic processes: a bleaching kinetics with a time constant of 60 ± 20 ns and a relative amplitude of 47% and an absorption kinetics with a time constant of 110 ± 20 ns and a relative amplitude of 53% fitted by a monoexponential kinetics. The combination of these two individual kinetics can well fit the experimental kinetics, which indicates that the breaking of the β-sheet occurs faster than its generation from the other secondary structure. Compared to the same band of T-jump at room temperature (Fig. 6), the dynamic feature is quite similar. However, at the higher temperature the formation of β-sheet dominates over its unfolding process. This is consistent with the fact that at a higher temperature more aggregated intermolecular β-sheet has been formed, since the β-sheet within an individual protein molecule is the precursor for the aggregated form.

Fig. 9 displays the bleaching kinetics at 1675 cm^{-1} for β-turn structure and an absorption kinetics at 1655 cm^{-1}, which can be assigned as the absorption from the loop structure rather than the helices, for even at a temperature above 50°C, the helical absorption remains at 1649 cm^{-1} for cyt *c*. When this bleaching kinetics is inverted to compare with that of the absorption as shown in the inset, both the kinetics are well matched with a time constant around 40 ns, i.e., 40 ± 10 ns at 1655 cm^{-1} and 35 ± 10 ns at 1675 cm^{-1}. Therefore, this pair of kinetics would correspond to the unfolding of the β-turn structure occurring simultaneously with the formation of a loop structure. It should be noted that the time constant for unfolding β-turn structures (1675 cm^{-1}) coincides well with the breaking of the β-sheet (1635 cm^{-1}, 60 ± 20 ns as shown in Fig. 8); therefore, it can be suggested that thermally induced unfolding of β-turn and β-sheet structure is a cooperative process. The assignments of the observed bands in both FTIR and the time-resolved IR spectra are summarized in Table 1.

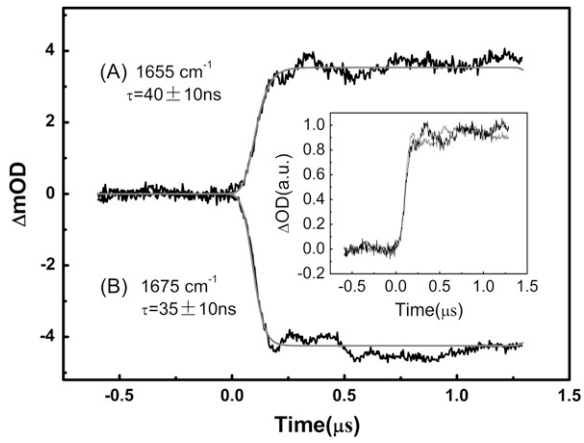

FIGURE 9 Kinetic IR response for a T-jump from 40°C to 50°C at (*A*) 1655 cm^{-1}, and (*B*) 1675 cm^{-1} (*solid black lines*). The solid shaded curves represent fits of the data to monoexponential kinetics convoluted with the instrument response function. The monoexpontial fittings yield time constants of 40 ± 10 ns and 35 ± 10 ns for the absorption and bleaching kinetics, respectively. (*Inset*) Superimposing of kinetic trace at 1655 cm^{-1} with the inverted trace at 1675 cm^{-1}.

The ω-loops investigated are segments along the polypeptide chain of cyt *c* with their two ends constrained by the neighboring structural units. However the loop structures can be viewed as the short polypeptide chains of the same residue sequence with special end caps. For the ω-loop with Met-80, we have shown that the T-jump at room temperature induces a loop to random coil transition. It is known that end caps and the peptide length can dramatically influence the thermodynamics of the helix-coil transition (39). Therefore an analogy can be made between the loop-coil and helix-coil transition. Recently, Gai's group has investigated the dependence of helix-coil transition kinetics on the end caps as well as the peptide length by the method of T-jump time-resolved difference IR absorbance spectra (39). They found that with T-jump from 25°C to 35°C, the unfolding time constant for the helix-coil transition is less dependent on the end caps and monotonically depends on the length of the peptide, i.e., from ~70 ns for a 19 residue peptide to ~170 ns for a 39-residue peptide.

Fast folding kinetics for a loop structure has also been investigated intensively in both theory (50,51) and experiments (52,53). The results show that the folding speed is limited by the rate of intramolecular contact formation or intrachain diffusion. This speed limit depends on the length of peptide separating the two contacting residues. Experimental measurement of the length dependence of an end-to-end contact rate for model peptides shows that the folding rate decreases from 1/(40 ns) for a separation of three residues to ~1/(140 ns) for a separation of 18 residues (53). Dyer and co-workers have measured the fast folding/unfolding kinetics in a T-jump-perturbed small 21-residue alanine-based model peptide by means of time-resolved IR absorbance difference spectra (54). They observed the model peptide exhibiting a fast unfolding of helix to coil kinetics with a time constant of 160 ± 60 ns at 28°C in response to a

TABLE 1 Assignment of the observed amide I′ band to its corresponding secondary structures

Observed (cm^{-1}) FTIR (T-jump)	Assignment	Literature values	References
1614	Intermolecular antiparallel β-sheets from aggregation	1614	43
1635 (1634)	β-sheet	1634 ~ 1635	44
1645	Random coil	1645 ~ 1647	41,42
1653 (1651, 1655)	α-Helix and loop	1650 ~ 1656	2,3,9–11
1674 (1675)	β-Turn	1674 ~ 1675	41,42
1684	Intermolecular antiparallel β-sheets from aggregation	1684 ~ 1685	43

T-jump of 18°C, which provides a limit speed for the unfolding of the secondary structure.

Kumar et al. recently investigated the ultrafast kinetics in the folding of the ferrocytochrome *c* by the use of laser flash photolysis and stop flow methods. They found that under the absolute refolding condition, the kinetics for intrapolypeptide making transient contacts with the heme iron in which the binding groups such as Met and His are brought to make a contact with heme Fe(II) by the chain diffusion to form a S-Fe or N-Fe bond have two distinct kinetic phases with a time constant of ~400 ns and 3 μs, respectively (31). These two kinetic phases are assigned to the transient binding of methonines (Met-80 and Met-65) and histidines (H-26 and H-33), respectively. It should be noted that in a similar experiment, Jones et al. have observed a 4 μs kinetic process assigned to the dissociation between the Met-80 and the heme group in the reduced cyt *c* (28), which is in agreement with the slower kinetic process observed by Kumar et al. In our T-jump experiment, the observed rate is a summation of the rates for transient contact and dissociation between the heme and Met-80.

As we have determined that the T_m of the loop-coil transition for the ω-loop containing Met-80 is ~45°C, the rate for the transient contact and dissociation would be the same at this temperature. We assume that the transient contact and dissociation would approximately have an equal rate at 36°C (T-jump from 25°C to 36°C); thus our observed time constant for dissociation of the iron-sulfur bond and transient contact between the heme and the Met-80 (loop diffusion) would be 280 ± 40 ns, which is consistent with that of the fast kinetic phase (~400 ns) probed for the transient contact between the heme and the Met-80 as reported in Kumar et al.'s work. In addition the unfolding time constant 60 ± 20 ns assigned to that of the folding/unfolding kinetics for the β-sheet and/or turns is close to the resolution limit of the instrument (~20 ns), indicating a much faster kinetic phase for the unfolding of the β-sheet or turns. It has been reported that the estimated time constant of making or breaking a single H-bond in a nucleated structure in a β-hairpin, referred to as the propagation time, is ~1 ns (55), and the disruption of β-sheet H-bonds in response to a T-jump has been reported to occur on a 1–5 ns timescale in ribonuclease A (32). Thus our results are in agreement with the literature values.

CONCLUSIONS

Due to the overlap of the amide I′ IR absorption band, band resolution and unambiguous assignment of the structural components can be difficult. Especially the loop absorption band is easily underscored when the helical secondary structures are also present. In this work, we investigated the FTIR spectra of horse cyt *c*, which consists of both helices and loops in D_2O under thermal perturbation. Furthermore T-jump time-resolved mid-IR absorbance difference spectra are used to investigate its thermal stability and folding/unfolding kinetics of the structural units. We distinguished the IR absorption band of a small ω-loop from that of the α-helices, i.e., the loop consists of residues 70–85 and binds to the heme Fe(III) through Met-80. Our results show that at room temperature both the loop and helical absorption bands overlap at 1653 cm^{-1}.

When raising the temperature, the absorption band at 1653 cm^{-1} shifts to 1649 cm^{-1} with an intensity loss. Thermal titration of the absorption intensity at this peak leads to a lower-temperature transition (T_m = 45°C), well before the global unfolding of the cyto *c* ($T_m \approx$ 82°C). This lower-temperature transition is assigned to the unfolding of the small ω-loop containing Met-80 in accompany with the thermal disruption of the S-Fe bond at the heme coordination site. T-jump time-resolved mid-IR absorbance difference spectra further show that the thermally induced unfolding process is a sequential process having several cooperative folding subunits characterized by their unfolding/folding time constants. At room temperature, a T-jump of 10°C induces an unfolding of the ω-loop with residues of 70–85 to a random coil with an observed time constant of 140 ± 20 ns. At a higher temperature of 40°C, a T-jump of 10°C would induce a cooperative unfolding of β-sheet (1635 cm^{-1}) and turn structures (1675 cm^{-1}) with a similar time constant, i.e., 60 ± 20 and 35 ± 10 ns.

We thank Prof. Qingxu Yu and Wang Zhang of Dalian University of Technology for their technical support in CO laser operation. We also thank Dr. H.W.Y. for help in preparation of the art work.

This work was supported by the National Natural Science Foundation of China (20373088) and Program for Innovation Group (60321002), Chinese Academy of Sciences innovative project (KJCX2-SW-w29), and National Key Project for Basic Research (2006CB910302).

REFERENCES

1. Krimm, S., and J. Bandekar. 1986. Vibrational spectroscopy and conformation of peptides, polypeptides, and proteins. *Adv. Protein Chem.* 38:181–364.
2. Susi, H., and D. M. Byler. 1986. Resolution-enhanced Fourier transform infrared spectroscopy of enzymes. *Methods Enzymol.* 130:290–311.
3. Surewicz, W. K., and H. H. Mantsch. 1988. New insight into protein secondary structure from resolution-enhanced infrared spectra. *Biochim. Biophys. Acta.* 952:115–130.
4. Arrondo, J. L. R., A. Muga, J. Castresana, and F. M. Goni. 1993. Quantitative studies of the structure of proteins in solution by Fourier-transform infrared spectroscopy. *Prog. Biophys. Mol. Biol.* 59:23–56.
5. Leeson, D. T., F. Gai, H. M. Rodriguez, L. M. Gregoret, and R. B. Dyer. 2000. Protein folding and unfolding on complex energy landscape. *Proc. Natl. Acad. Sci. USA.* 97:2527–2532.
6. Kauppinen, J. K., D. J. Moffatt, H. H. Mantsch, and D. G. Cameron. 1981. Fourier self-deconvolution: a method for resolving intrinsically overlapped bands. *Appl. Spectrosc.* 35:271–276.
7. Cameron, D. G., J. K. Kauppinen, D. J. Moffatt, and H. H. Mantsch. 1982. Precision in condensed phase vibrational spectroscopy. *Appl. Spectrosc.* 36:245–250.
8. Cameron, D. G., and D. J. Moffatt. 1984. Deconvolution, derivation, and smoothing of spectra using Fourier transforms. *J. Test. Eval.* 12:78–85.

9. Filosa, A., Y. A. Wang, A. Ismail, and A. M. English. 2001. Two-dimensional infrared correlation spectroscopy as a probe of sequential events in the thermal unfolding of cytochrome *c*. *Biochemistry*. 40: 8256–8263.
10. Bowler, B. E., J. A. Dong, and W. S. Caugheys. 1994. Characterization of the guanidine hydrochloride-denatured state of iso-1-cytochrome *c* by infrared spectroscopy. *Biochemistry*. 33:2402–2408.
11. Wilder, C. L., A. D. Friedrich, R. O. Potts, G. O. Daumy, and M. L. Francoeur. 1992. Secondary structural analysis of two recombinant murine proteins, interleukins 1α and lβ: is infrared spectroscopy sufficient to assign structure? *Biochemistry*. 31:27–31.
12. Milne, J. S., Y. J. Xu, L. C. Mayne, and S. W. Englander. 1999. Experimental study of the protein folding landscape: unfolding reactions in cytochrome *c*. *J. Mol. Biol.* 290:811–822.
13. Kaminsky, L. S., V. J. Miller, and A. J. Davison. 1973. Thermodynamic studies of opening of heme crevice of ferricytochrome *c*. *Biochemistry*. 12:2215–2221.
14. Schejter, A., T. L. Luntz, T. I. Koshy, and E. Margoliash. 1992. Relationship between local and global stabilities of proteins: site-directed mutants and chemically-modified derivatives of cytochrome *c*. *Biochemistry*. 31:8336–8379.
15. Hu, Y. Z., C. Fenwick, and A. M. English. 1996. Local stabilities of horse cytochrome *c* metalloderivatives as probed by tryptic digestion and electrospray mass spectrometry. *Inorg. Chim. Acta*. 242: 261–269.
16. Bushnell, G. W., G. V. Louie, and G. D. Brayer. 1990. High-resolution three-dimensional structure of horse heart cytochrome *c*. *J. Mol. Biol.* 214:585–595.
17. Dong, A. C., P. Huang, and W. S. Canghey. 1990. Protein secondary structure in water from second-derivative amide I infrared spectra. *Biochemistry*. 29:3303–3308.
18. Dong, A., P. Huang, and W. S. Caughey. 1992. Redox-dependent changes in β-extended chain and turn structures of cytochrome *c* in water solution determined by second derivative amide I infrared spectra. *Biochemistry*. 31:182–189.
19. Banci, L., I. Bertini, H. B. Gray, C. Luchinat, T. Reddig, A. Rosato, and P. Turano. 1997. Solution structure of oxidized horse heart cytochrome *c*. *Biochemistry*. 36:9867–9877.
20. Margoliash, E., and A. Schejter. 1966. Cytochrome *c*. *Adv. Protein Chem.* 21:113–286.
21. Daidone, I., A. Amadei, D. Roccatano, and A. D. Nola. 2003. Molecular dynamics simulation of protein folding by essential dynamics sampling: folding landscape of horse heart cytochrome *c*. *Biophys. J.* 85:2865–2871.
22. Elove, G. A., A. K. Bhuyan, and H. Roder. 1994. Kinetic mechanism of cytochrome *c* folding: involvement of the heme and its ligands. *Biochemistry*. 33:6925–6935.
23. Hoang, L., S. Bedard, M. M. G. Krishna, Y. Lin, and S. W. Englander. 2002. Cytochrome *c* folding pathway: kinetic native-state hydrogen exchange. *Proc. Natl. Acad. Sci. USA*. 99:12173–12178.
24. Bai, Y., T. R. Sosnick, L. Mayne, and S. W. Englander. 1995. Protein folding intermediates studied by native state hydrogen exchange. *Science*. 269:192–197.
25. Filosa, A., and A. M. English. 2000. Probing local thermal stabilities of bovine, horse, and tuna ferricytochromes *c* at pH 7. *J. Biolog. Inorg. Chem.* 5:448–454.
26. Filosa, A., A. A. Ismail, and A. M. Engliah. 1999. FTIR-monitored thermal titration reveals different mechanisms for the alkaline isomerization of tuna compared to horse and bovine cytochromes *c*. *J. Biolog. Inorg. Chem.* 4:717–726.
27. Yeh, S.-R., and D. L. Rousseau. 2002. Hierarchical folding of cytochrome *c*. *Nat. Struct. Biol.* 7:443–445.
28. Jones, C. M., E. R. Henry, Y. Hu, C. K. Chan, S. D. Luck, A. Bhuyan, H. Roder, J. Hofrichter, and W. A. Eaton. 1993. Fast events in protein folding initiated by nanosecond laser photolysis. *Proc. Natl. Acad. Sci. USA*. 90:11860–11864.
29. Goldbeck, R. A., Y. G. Thomas, E. Chen, R. M. Esquerra, and D. S. Kliger. 1999. Multiple pathways on a protein-folding energy landscape: kinetic evidence. *Proc. Natl. Acad. Sci. USA*. 96:2782–2787.
30. Andinrud, P. A., C. Han, and R. M. Hochstrasser. 1989. Direct observation of ligand dynamics in hemoglobin by subpicosecond infrared spectroscopy. *Proc. Natl. Acad. Sci. USA*. 86:8387–8391.
31. Kumar, R., N. P. Prabhu, and A. K. Bhuyan. 2005. Ultrafast events in the folding of ferrocytochrome *c*. *Biochemistry*. 44:9359–9367.
32. Phillips, C. M., Y. Mizutani, and R. M. Hochstrasser. 1995. Ultrafast thermally induced unfolding of RNase A. *Proc. Natl. Acad. Sci. USA*. 92:7292–7296.
33. Dyer, R. B., F. Gai, W. H. Woodruff, R. Gilmanshin, and R. H. Callender. 1998. Infrared studies of fast events in protein folding. *Acc. Chem. Res.* 31:709–716.
34. Callender, R., and R. B. Dyer. 2006. Advances in time-resolved approaches to characterize the dynamical nature of enzymatic catalysis. *Chem. Rev.* 106:3031–3042.
35. Wright, W. W., M. Laberge, and J. M. Venderkooi. 1997. Surface of cytochrome *c*: infrared spectroscopy of carboxyl groups. *Biochemistry*. 36:14724–14732.
36. Chalikian, T. V., V. S. Gindikin, and K. J. Breslauer. 1996. Spectroscopic and volumetric investigation of cytochrome *c* unfolding at alkaline pH: characterization of the base-induced unfolded state at 25°C. *FASEB J.* 10:164–170.
37. Susi, H., and D. M. Byler. 1983. Protein structure by Fourier transform infrared spectroscopy: second derivative spectra. *Biochem. Biophys. Res. Commun.* 115:391–397.
38. Zhang, Q. L., L. Wang, Y. X. Weng, X. G. Qiu, W. C. Wang, and J. X. Yan. 2005. Nanosecond-time-resolved infrared spectroscopic study of fast relaxation kinetics of protein folding by means of laser-induced temperature-jump. *Chin. Phys.* 14:2484–2490.
39. Wang, T., Y. Zhu, Z. Getahun, D. Du, C.-Y. Huang, W. DeGrado, and F. Gai. 2004. Length dependent helix-coil transition kinetics of nine alanine-based peptides. *J. Phys. Chem. B*. 108:15301–15310.
40. Huang, C.-Y., Z. Getahun, Y. Zhu, J. W. Klemke, W. F. DeGrado, and F. Gai. 2002. Helix formation via conformation diffusion search. *Proc. Natl. Acad. Sci. USA*. 99:2788–2793.
41. Prestrelski, S. J., D. M. Byler, and M. P. Thompson. 1991. Infrared spectroscopic discrimination between alpha- and $3(_{10})$-helices in globular proteins. Reexamination of amide I infrared bands of alpha-lactalbumin and their assignment to secondary structures. *Int. J. Pept. Protein Res.* 37:508–512.
42. Prestrelski, S. J., D. M. Byler, and M. P. Thompson. 1991. Effect of metal ion binding on the secondary structure of bovine alpha-lactalbumin as examined by infrared spectroscopy. *Biochemistry*. 30:8797–8804.
43. Ismail, A. A., H. H. Mantsch, and P. T. Wong. 1992. Aggregation of chymotrypsinogen: portrait by infrared spectroscopy. *Biochim. Biophys. Acta*. 1121:183–188.
44. Holzbaur, I. E., A. M. English, and A. A. Ismail. 1996. FTIR study of the thermal denaturation of horseradish and cytochrome *c* peroxidases in D_2O. *Biochemistry*. 35:5488–5494.
45. Muga, A., H. H. Mantsch, and W. K. Surewicz. 1991. Membrane binding induces destabilization of cytochrome *c* structure. *Biochemistry*. 30:7219–7224.
46. Taler, G., A. Schejyler, G. Navon, I. Vig, and E. Margoliash. 1995. The nature of the thermal equilibrium affecting the iron coordination of ferric cytochrome *c*. *Biochemitry*. 34:14209–14212.
47. Gilmanshin, R., S. Williams, R. H. Callender, W. H. Woodruff, and R. B. Dyer. 1997. Fast events in protein folding: relaxation dynamics of secondary and tertiary structure in native apomyoglobin. *Proc. Natl. Acad. Sci. USA*. 94:3709–3713.
48. Schmid, F. X. 1992. Kinetics of unfolding and refolding of single-domain proteins. *In* Protein Folding. T. E. Creighton, editor. W. H. Freeman, New York. 197–241.

49. Speare, J. O., and T. S. Rush. 2003. IR spectra of cytochrome *c* denatured with deuterated guanidine hydrochloride show increase in β-sheet. *Biopolymers*. 72:193–204.

50. Camacho, C. J., and D. Thirumalai. 1995. Theoretical predictions of folding pathways by using the proximity rule, with applications to bovine pancreatic trypsin inhibitor. *Proc. Natl. Acad. Sci. USA*. 92: 1277–1281.

51. Thirumalai, D. 1999. Time scales for the formation of the most probable tertiary contacts in proteins with applications to cytochrome *c*. *J. Phys. Chem. B*. 103:608–610.

52. Bieri, O., J. Wirz, B. Hellrung, M. Schutkowski, M. Drewello, and T. Kiefhaber. 1999. The speed limit for protein folding measured by triplet-triplet energy transfer. *Proc. Natl. Acad. Sci. USA*. 96:9597–9601.

53. Lapidus, L. J., W. A. Eaton, and J. Hofrichter. 2000. Measuring the rate of intramolecular contact formation in polypeptides. *Proc. Natl. Acad. Sci. USA*. 97:7220–7225.

54. Williams, S., T. P. Causgrove, R. Gilmanshin, K. S. Fang, R. H. Callender, W. H. Woodruff, and R. B. Dyer. 1996. Fast events in protein folding: helix melting and formation in a small peptide. *Biochemistry*. 35:691–697.

55. Muńoz, V., P. Thompson, J. Hofrichter, and W. A. Eaton. 1997. Folding dynamics and mechanism of β-hairpin formation. *Nature*. 390:196–199.